

Designing Ultra-Low Hydrate Adhesion Surfaces by Interfacial Spreading of Water-Immiscible Barrier Films

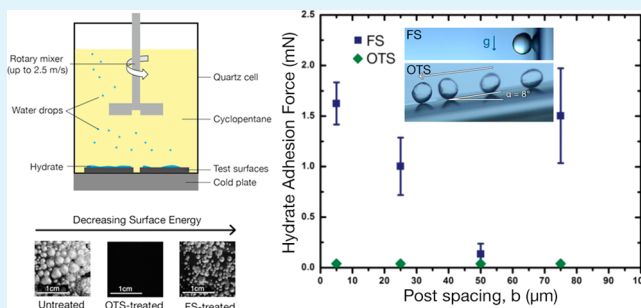
Arindam Das, Taylor A. Farnham,[†] Srinivas Bengaluru Subramanyam,[‡] and Kripa K. Varanasi*

Department of Mechanical Engineering, Massachusetts Institute of Technology, 77 Massachusetts Ave., Cambridge, Massachusetts 02139, United States

Supporting Information

ABSTRACT: Clathrate hydrates are icelike solid substances that can form inside oil and gas pipelines and are responsible for flow blockages, sometimes leading to catastrophic failures. Minimizing hydrate formation and adhesion on pipeline surfaces can effectively address this problem. In this paper, we achieve the lowering of the adhesion of cyclopentane hydrates by promoting a cyclopentane barrier film between the hydrate and solid surface. The presence of this interfacial liquid film depends on the relative spreading of cyclopentane on the solid surface in the presence of water. We study the role of surface chemistry and surface texture on the spreading characteristics of such interfacial films and their impact on hydrate adhesion. The use of the spreading coefficients as design parameters could take us a step closer to the development of effective passive antihydrate surfaces.

KEYWORDS: clathrate hydrate, adhesion, surface energy, spreading coefficient, interfacial spreading



INTRODUCTION

Clathrate hydrates are solid, crystalline materials that consist of a cage of hydrogen-bonded water molecules encasing one or more guest molecules.¹ These materials have been found to be valuable sources of energy and are potential candidates for use in energy storage.^{2,3} However, clathrate hydrates have proven to be an impediment to pipe flow in the oil and gas industry where the high pressure and low temperature conditions are conducive to their formation.⁴ They may restrict or plug flowlines,⁴ halting production and potentially rupturing pipes and equipment, sometimes fatally.⁵ Current methods of hydrate mitigation, including the use of chemical additives and heating of pipe walls, are energy-intensive and in many cases environmentally unfriendly.^{1,6,7}

Clathrate hydrates encompass a wide family and contain a variety of guest molecules (i.e., hydrate formers), such as methane, ethane, propane, carbon dioxide, tetrahydrofuran, and cyclopentane.^{4,8–10} Given the relevance and potential of clathrate hydrates, a significant amount of work has been devoted to understanding their structure and the dynamics of their formation.¹ There has also been a focus on reducing hydrate adhesion on surfaces to prevent hydrate plugs and blockages.^{11–20} It has been shown recently that the surface chemistry of the solid plays an important role in determining the adhesion of hydrates to that solid.^{12,15–17,19} The dependence of hydrate cohesion and adhesion on the interfacial tension between the hydrate former and water has also been studied.¹⁷ However, the three-phase interactions between the hydrate former, water, and the solid substrate and their

subsequent effect on hydrate adhesion have not yet been considered.

While methane hydrates are highly prevalent in the oil and gas industry, the extreme conditions required for their formation (minimum pressure of 2–6 MPa at 0–10 °C) often necessitate the use of a model clathrate hydrate system for laboratory studies. Cyclopentane hydrates, with a critical temperature of 7.7 °C at ambient pressures and SII crystalline structure are often used as a model system.²¹ The critical temperature for their formation is sufficiently above the freezing point of water, thereby avoiding ice contamination in the experiments.

Figure 1 demonstrates cyclopentane hydrate accumulation on substrates with varying surface chemistries at 5 °C. The schematic of the experimental setup for studying hydrate accumulation is also shown in Figure 1. See the experimental section for further details. The bare silicon surface (surface energy $\sim 53 \text{ mJ m}^{-2}$)²² shows the highest hydrate accumulation with a combination of large hydrate clusters and a thin hydrate layer covering the remaining surface. The two silane-modified surfaces [octadecyltrichlorosilane (OTS) and tridecafluoro-1,1,2,2-tetrahydrooctyl-trichlorosilane (FS)] show substantially less hydrate formation, consistent with their low surface energies. However, contrary to conventional wisdom, the FS-coated surface with the lowest surface energy ($\sim 8 \text{ mJ m}^{-2}$) has

Received: January 5, 2017

Accepted: March 10, 2017

Published: March 10, 2017

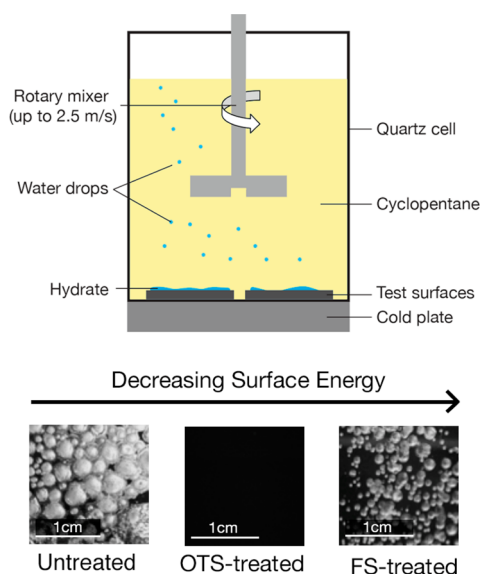


Figure 1. Hydrate accumulation setup and hydrate accumulation on smooth untreated, OTS-treated, and FS-treated surfaces.

a larger coverage of hydrate crystals compared to an OTS-coated surface with a higher surface energy ($\sim 24 \text{ mJ m}^{-2}$).

This unexpected behavior inspired us to further study the role of the interfacial interactions between the solid substrate, water, and cyclopentane during hydrate accumulation. We find that the spreading coefficient of the water immiscible liquid phase (here cyclopentane) effectively captures the influence of the three-phase interfacial interactions on hydrate formation and adhesion on both smooth and textured surfaces.

RESULTS AND DISCUSSION

Water Contact Angle and Cyclopentane Spreading Coefficient. Water and cyclopentane are the precursors for cyclopentane hydrates, and their wettabilities can be used to compare hydrate formation and adhesion on different surfaces. Static, advancing, receding, and roll-off angles of $3 \mu\text{L}$ water droplets in the presence of cyclopentane on untreated, OTS-treated, and FS-treated silicon surfaces are tabulated in Table 1.

Contact angle hysteresis, the difference between advancing and receding contact angles, is a measure of the attraction between a liquid and the underlying solid surface, with greater hysteresis indicating greater pinning and higher roll-off angles. The contact angle hysteresis of water on the untreated and FS-treated surfaces in cyclopentane is $\sim 24^\circ$ and $\sim 55^\circ$, respectively. As a result, a water droplet sticks to these surfaces even at a 90° tilt angle. On the OTS-treated surface, however, the water contact angle hysteresis is much lower than those on untreated and FS-treated surfaces, and water drops roll off at only 2° inclination. The negligible hysteresis and roll-off angles indicate the presence of a thin film of cyclopentane under the water drop on OTS-treated surfaces. In other words, the spreading coefficient of cyclopentane on the surface in the water

environment, $S_{\text{os(w)}}$, is positive for OTS-treated surfaces and negative for FS-treated and untreated surfaces. The expression for the spreading coefficient is given by equation 1,

$$S_{\text{os(w)}} = \gamma_{\text{sw}} - \gamma_{\text{os}} - \gamma_{\text{wo}} \quad (1)$$

where γ is the interfacial tension between the two subscripted phases: solid (s), water (w), and cyclopentane (o).

The two regimes of the spreading coefficient of cyclopentane are shown in Figure 2. The positive spreading coefficient of

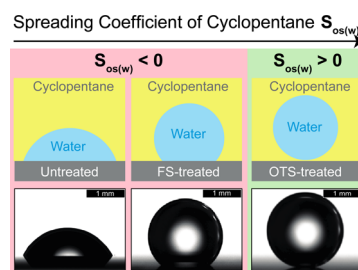


Figure 2. Schematic and images of water contact angles on solid surfaces corresponding to the two regimes of the spreading coefficient $S_{\text{os(w)}}$ of cyclopentane (o) on a solid (s) in the presence of water (w).

cyclopentane on OTS-treated surfaces causes water to bead up into perfectly spherical drops that are extremely mobile on the surface (see video S1) due to rapid spreading of cyclopentane on OTS in water (see video S2). The thin cyclopentane film underneath the water drops acts as a barrier, limiting the contact area of water and hydrate with the underlying solid. This thin film forms due to the high chemical affinity of OTS terminal groups [$-\text{CH}_3$] to cyclopentane ($-\text{CH}_2$ groups). The $-\text{CH}_3$ group on the OTS surface is nonpolar (the electronegativity difference between a carbon and hydrogen atom is 0.35 eV, and the dipole moment is less than 0.40 D)²³ and thus has limited interaction with water. On the other hand, the negative spreading coefficient of cyclopentane on untreated and FS-treated surfaces results in greater interaction between the solid surface and water and results in lower water contact angles in the cyclopentane environment (Figure 2 and Table 2). This

Table 2. Advancing and Receding Contact Angles of Cyclopentane in the Presence of Water

	advancing angle	receding angle
untreated	$125^\circ \pm 3^\circ$	$102^\circ \pm 3^\circ$
FS-treated	$45^\circ \pm 3^\circ$	$23^\circ \pm 1^\circ$
OTS-treated	0°	0°

is further evident by the clear depinning of the cyclopentane layer within the water environment (see video S3). Increased polarity (electronegativity difference = 1.78 eV and dipole moment $\sim 1.51 \text{ D}$ for the C–F bond) of fluorinated groups present on the FS surface can be held responsible for higher surface water interaction. Eventually, this leads to greater

Table 1. Static Contact Angles, Dynamic Contact Angles and Roll-off Angles of Water Drops ($3 \mu\text{L}$) in Cyclopentane

	advancing angle	receding angle	static contact angle	contact angle hysteresis	roll-off angle
untreated	$78^\circ \pm 4^\circ$	$54^\circ \pm 4^\circ$	$59^\circ \pm 2^\circ$	$\sim 24^\circ$	$>90^\circ$ (sticks)
FS-treated	$153^\circ \pm 4^\circ$	$99^\circ \pm 5^\circ$	$138^\circ \pm 3^\circ$	$\sim 55^\circ$	$>90^\circ$ (sticks)
OTS-treated	$164^\circ \pm 2^\circ$	$163^\circ \pm 2^\circ$	$163^\circ \pm 2^\circ$	$\sim 1^\circ$	$<2^\circ$ (slides)

hydrate formation on untreated and FS-treated surfaces as shown in Figure 1.

Hydrate Growth on Solid Surfaces of Varying Surface Energy. The changes in the interfacial contact area associated with the formation of a hydrate crystal on the solid–water interface determine its degree of adhesion to a solid surface. The adhesion strength depends on the surface chemistry and the contact area between the hydrate and the solid surface. Figure 3 shows the sequence of the growth of hydrate on the

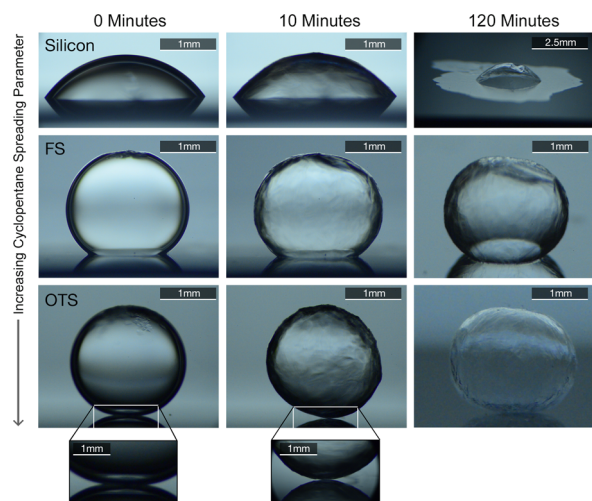


Figure 3. Sequences of hydrate growth from chilled water droplets submerged in cyclopentane on solid surfaces of varied interfacial surface energies. Preformed hydrate crystals were introduced to initiate the hydrate growth.

three different surfaces used in this work. Hydrate seed crystals are used to initiate the nucleation of hydrate in a liquid water droplet placed in a cyclopentane bath at 1 °C. See the experimental section for further details.

On the untreated silicon surface, a thin white solid hydrate layer grows outward from the three-phase contact line and eventually covers the entire surface. By expanding beyond the initial contact area, this thin layer is expected to further increase the hydrate adhesion to the solid surface. On the other hand, during the hydrate formation on the OTS-coated surface, the interfacial contact area is reduced to essentially a single point contact (Figure 3 inset). Moreover, during the formation process, the droplet is observed to slide and rotate on the OTS-coated surface (see Video S4 and Video S5). Lastly, on the FS-treated surface, the hydrate maintains roughly the same contact area as the initial water droplet.

The importance of the changes in the interfacial contact area observed previously at the solid–water interface is emphasized in the surface tilt experiments. Once the hydrate crystals nucleate on the surface, the solid substrates are gradually tilted from 0° to 90°. A poorly adhered crystal is expected to slide and fall under its own weight at some critical tilt angle, while strong adhesion would ensure the retention of the hydrate on the surface even at maximum inclination. Figure 4 shows the results of these experiments on untreated, FS-coated, and OTS-coated silicon surfaces.

The formation of the thin hydrate layer covering the entire substrate on the untreated silicon surface results in a high adhesion strength such that even a 90° inclination is insufficient for the crystal to detach. On the FS-coated surface, the finite interfacial contact area results in hydrate retention even at a 90°

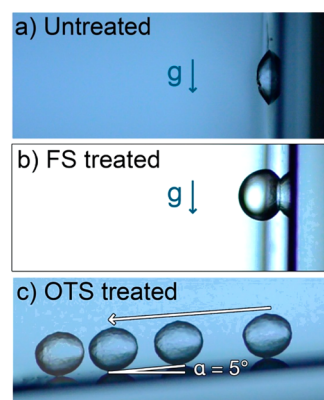


Figure 4. Hydrate adheres to (a) untreated silicon and (b) FS-treated silicon up to 90° inclination; movement begins on the (c) OTS-treated silicon at approximately 5° inclination.

inclination. This is consistent with the absence of a barrier film of cyclopentane on FS and the hydrate crystal being in intimate contact with the solid surface. The OTS-treated surface shows remarkably less adhesion, and the hydrate slides off the surface at approximately 5° inclination. The effect of the barrier film of cyclopentane on OTS is supplemented by the changes in the hydrate–substrate interfacial contact area during hydrate formation, resulting in limited contact with the surface (Figure 3). This result validates the necessity of the spreading coefficient of cyclopentane to be positive to achieve the lowest possible hydrate adhesion.

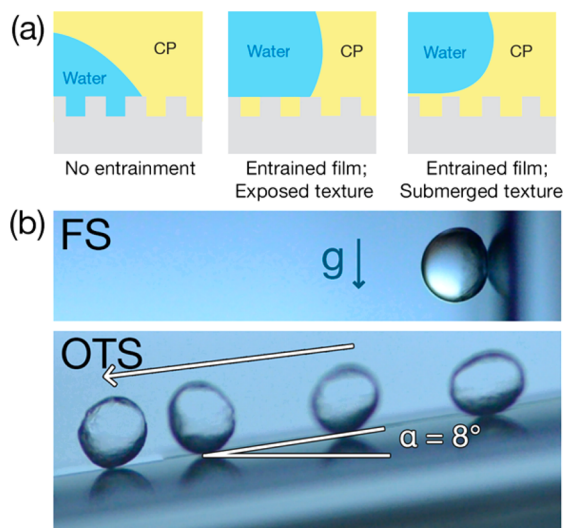
Thermodynamic Stability of Cyclopentane within Rough Surfaces and Hydrate Adhesion. Real surfaces are rarely smooth, and the results observed previously have to be extended to rough surfaces for any practical relevance. Here we study the effect of surface roughness on the presence of the cyclopentane barrier film and its wetting properties. We textured each surface using photolithography to obtain square microposts of 10 μm side length, 10 μm depth, and varied the spacing between microposts. The entrainment of cyclopentane within the surface features underneath the water drop depends on both the surface chemistry and the geometry of the surface texture. For the thermodynamic stability of the entrained film within the surface texture, the contact angle of cyclopentane in the presence of water ($\theta_{os(w)}$) on a smooth surface with the same surface chemistry has to be less than a critical angle $\theta_c \equiv \cos^{-1} [(1 - \phi)/(r - \phi)]$, where ϕ is the projected solid fraction and r is the roughness ratio.^{24,25}

For the samples studied here with square microposts of length a , depth h , and spacing b , these parameters are defined as $\phi \equiv [a^2/(a + b)^2]$ and $r \equiv 1 + [4ah/(a + b)^2]$. While $\theta_{os(w)}$ depends on the surface chemistry, θ_c is purely a function of the surface geometry. Table 2 shows the dynamic contact angles of cyclopentane on different surfaces in water. The values of the critical contact angle θ_c are tabulated in Table 3 for the different geometries of the surface texture used here.

When textured surfaces are immersed in a cyclopentane bath with water drops placed on top of them, the surfaces may exist in three different states: a water impaled state, a cyclopentane entrained state with the texture tops exposed, and a cyclopentane entrained state with the entire texture submerged (Figure 5a). On OTS-treated surfaces, a zero receding angle indicates successful entrainment of cyclopentane within the surface features ($\theta_{os(w)} < \theta_c$) and submergence of the texture because of the positive spreading coefficient ($\theta_{os(w)} = 0$). This

Table 3. Geometric Parameters on Different Textures with $a = 10 \mu\text{m}$, $h = 10 \mu\text{m}$

b (μm)	ϕ	r	θ_c
5	0.44	2.78	76°
25	0.08	1.33	42°
50	0.03	1.11	26°
75	0.01	1.06	19°

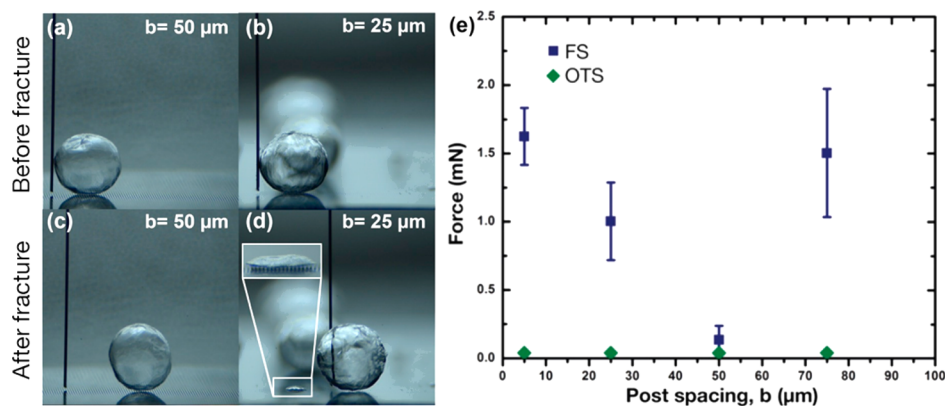
**Figure 5.** (a) Schematic of the thermodynamic states of a textured surface placed in cyclopentane with a water drop on top. (b) Tilt experiments showing hydrate retention on textured surfaces with $5 \mu\text{m}$ post spacing. The hydrate on the FS-treated surface remains even at 90° inclination, while the hydrate moves at 8° tilt on OTS-treated surfaces.

phenomenon is observed for all geometries, and a barrier film is present to prevent any hydrate stiction. Figure 5b validates this hypothesis with the hydrate particle sliding on the OTS-treated textured surface at a tilt angle of just 8° because of poor adhesion to the surface.

By contrast, the adhesion of hydrate to FS-treated rough surfaces is high. The entrainment of cyclopentane within the texture depends on the surface geometry of FS-treated surfaces. Here, we suggest that the receding contact angle (rather than the equilibrium contact angle) has to satisfy the entrainment

criterion ($\theta_{\text{os(w)}} < \theta_c$) to prevent cyclopentane dewetting and subsequent impalement of the water drop. As shown in Table 3, for all surface geometries with ($\theta_{\text{os(w)}} < \theta_c$), the entrainment of cyclopentane within the surface features occurs as confirmed by optical images and roll-off angles (see the Supporting Information), although the texture tops remain exposed to water because of the negative spreading coefficient of cyclopentane. The surface tilt experiments in Figure 5b show the high stiction of the hydrate crystal on a FS-treated textured surface with $5 \mu\text{m}$ post spacing, even at a 90° tilt angle.

To further quantify the adhesion of hydrate on textured FS-treated and OTS-treated surfaces, a thin steel wire is used as a cantilever to dislodge the hydrates from the surface. The adhesion forces are calculated from the deflection of the wire and its effective elastic modulus. In most cases, the hydrate fails adhesively and no residual hydrate remains on the surface (Figure 6, panels a and c). However, on FS-treated surfaces with either 5 or $75 \mu\text{m}$ post spacing, as well as on some FS-treated surfaces with $25 \mu\text{m}$ post spacing, the hydrate fails cohesively and a portion of the hydrate crystal remains on the surface (Figure 6, panels b and d). In such cases of cohesive fracture, the maximum deflection of the cantilever before cohesive failure is used as a conservative lower bound for the adhesive force calculation. Hydrate adhesion forces on FS-treated and OTS-treated forces are plotted in Figure 6e for different interpost separations. Textured FS-treated surfaces show greater adhesion than corresponding textured OTS-treated surfaces, consistent with the results of the surface tilt experiments. The adhesion force on textured FS-treated surfaces initially decreases as interpost spacing is increased from 5 to $50 \mu\text{m}$, followed by a sudden increase in adhesion at $75 \mu\text{m}$. As one may expect, increasing the interpost spacing decreases the density of microposts and reduces the area available for hydrate adhesion. With the tops of the texture of the FS-treated surfaces exposed and a possible crystallization of the hydrate into the entrained cyclopentane film, increasing interpost spacing corresponds to decreasing the interfacial contact area; that is, there is less solid area available for the hydrate to adhere. The extent of the hydrate growth into the roughness features of the FS-treated surfaces is still unclear, and further experiments are needed to investigate this thoroughly. For the interpost spacing of $75 \mu\text{m}$, as indicated in Tables 2 and 3, ($\theta_{\text{os(w)}} < \theta_c$) and cyclopentane is no longer entrained within the texture. This increases the interfacial contact area between

**Figure 6.** (a–d) Steel cantilever wire used to dislodge the hydrate particles from test surfaces. Hydrate particles are dislodged either (a and c) adhesively or (b and d) cohesively. Inset of (d) shows hydrate residue, which remains on the surface after cohesive fracture. (e) shows a plot of adhesion forces as a function of post spacing on both OTS and FS-treated surfaces.

the hydrate and the solid surface, thereby increasing hydrate adhesion.

OTS-treated surfaces show about 2 orders of magnitude lower adhesion than FS-treated surfaces for all the interpost separations. The highest adhesion strength observed on the textured sample with 5 μm interpost spacing was just about 0.02 mN, while on the textures with higher post separations, hydrates were dislodged without any observed deflection of the steel cantilever, indicating adhesion forces less than 0.004 mN, the lower limit of the experiment.

CONCLUSIONS

The spreading coefficient has been proposed as a predictor of hydrate formation and adhesion in place of conventional surface energy measurements. Smooth and textured silicon samples were treated with either FS or OTS and used to measure hydrate accumulation and adhesion. Despite the significantly lower surface energy of FS-coated surfaces, the OTS-coated samples consistently showed less hydrate accumulation and almost zero adhesive strength. While surface energy predictions were consistent with the poor performance of untreated silicon, the spreading coefficient of cyclopentane on the solid in water accurately captured the full range of performance across all samples. For a positive spreading coefficient of cyclopentane, the solid–water contact area dramatically shrank with the formation of a cyclopentane barrier film, which results in greatly reduced hydrate accumulation and adhesion. As such, the OTS-coated samples have shown near-zero accumulation and a 2 orders of magnitude reduction in adhesion when compared to FS-coated samples. These results suggest that an optimal design of the surface chemistry of the solid surface can promote the formation of a barrier film and provide passive minimization of hydrate accumulation and adhesion.

Similar to gas hydrates, cyclopentane hydrates form at an immiscible oil (cyclopentane)–water interface characterized by the low solubility of the hydrate forming phase (cyclopentane) in water. In oil–water systems, the hydrate-forming gases and molecules are dissolved in the oil phase and the hydrate forms at the oil–water interface. Similarly, in gas-dominated flow the hydrate forms at the interface between the gas and condensed water droplets. While the high pressure presents vastly different challenges for hydrate adhesion reduction, understanding the fundamentals of the interfacial interactions between the solid substrate and the hydrate structure is a good first step in designing surfaces that function even under high pressure. Upon the basis of the results reported here, we anticipate that allowing the complete spread of nonaqueous, water-immiscible films on solid surfaces will reduce gas hydrate adhesion, even under high pressure condition; however, further study is warranted.

EXPERIMENTAL METHODS

Surface Functionalization. Six-inch silicon wafers were cut to approximately 20 mm squares by a 1064 nm Nd:YAG laser (Electrox). The samples were coated with OTS (octadecyltrichlorosilane, Sigma-Aldrich) or FS (tridecafluoro-1,1,2,2 tetrahydrooctyl-trichlorosilane, Sigma-Aldrich) through liquid and vapor deposition, respectively. For OTS deposition, samples were first plasma cleaned for 10 min and then placed in a mixture of 75 mL toluene and 250 μL OTS. To this mixture, an emulsion of 325 μL deionized water (Millipore, 18.2M Ω) and 50 mL toluene was added. The water-in-toluene emulsion was prepared by 90 s of rigorous mixing through high-energy probe sonication (Sonics 750W sonicator). The new mixture was bath-

sonicated (Branson) for 2 min. After at least 20 min in the reactive solution, excess OTS was removed from the sample by rinsing with acetone and isopropanol. FS deposition was achieved by first plasma cleaning samples for 10 min and placing the samples in a vacuum desiccator with 10 μL FS. The desiccator was purged and held to vacuum for 4 h; excess FS was removed by rinsing and sonicating for 3 min with acetone and isopropanol.

Surface Texturing. Microtextured silicon surfaces with periodic 10 μm square posts, interpost spacings of 5, 25, 50, and 75 μm , and heights of 10 μm were fabricated by a standard lithographic process. Lithography was performed by coating wafers with Shipley S1818 photoresist, selectively exposing them to 405 nm wavelength ultraviolet light using a chrome mask (Advance Reproductions Corporations), developing the photoresist in 1:1 volume ratio of DI water and Microdev solution (Dow Chemicals), and etching (inductively coupled plasma reactor, Surface Technology Systems) the silicon to a depth of 10 μm . Surface profilometry was performed using an optical profiler (CCI HD Optical Profiler, Taylor Hobson) followed by removing the remaining photoresist in a piranha solution (3:1 volume ratio of sulfuric acid and hydrogen peroxide).

Contact Angle and Surface Energy Measurement. Advancing and receding contact angles of water in air and cyclopentane environments were measured using a Ramé-Hart M500 goniometer. For the cyclopentane environment, the sample was submerged in a transparent quartz cell filled with cyclopentane. For the contact angle of cyclopentane in water, an L-shaped needle was used to dispense the cyclopentane drops and the sample was placed inverted in a water bath, since cyclopentane is less dense and floats on water. Drops of 5 μL DI water were dispensed and retracted at a rate of 0.2 $\mu\text{L/s}$, and advancing and receding water contact angles were recorded, respectively. At least ten measurements were performed on each sample, and the average and standard deviation values are reported. The surface energies of the FS-treated and OTS-treated smooth substrates were calculated via the Van Oss-Chaudury-Good approach, as described elsewhere,^{26,27} using 3 probe liquids (water, ethylene glycol, and diiodomethane).

Hydrate Accumulation. Hydrate formation under rotary mixing was used to assess hydrate accumulation. Samples were placed in a transparent quartz cell filled with cyclopentane. The system was placed atop a Peltier chiller (Stir Kool) and was chilled to $-5\text{ }^\circ\text{C}$ and held for 15 min. A mechanical mixer was inserted into the bath and rotated at 200 rpm. A 36-gauge needle was used to dispense a total of 0.3 mL of water as droplets of approximately 100 μm diameter into the bath at a rate of 1 mL min^{-1} . The cyclopentane bath temperature was then cycled between -5 and $5\text{ }^\circ\text{C}$ at $1\text{ }^\circ\text{C min}^{-1}$ for 30 min to initiate the nucleation of hydrate at the interface of ice and cyclopentane. The bath temperature was ultimately held at $5\text{ }^\circ\text{C}$, above the freezing point of water, for 90 additional minutes to ensure no ice contamination.

Hydrate Formation for Adhesion Force Measurement. Seed crystals of preformed hydrate were used to initiate hydrate nucleation for the adhesion measurements. Samples were placed in a transparent quartz cell filled with cyclopentane. Water droplets with a volume of 3 μL were added, and the test chamber was chilled to $1\text{ }^\circ\text{C}$ via Peltier chiller (Stir Kool). A 100 μm diameter steel wire (Hamilton Co.) was used to introduce hydrate seed crystals to the chilled water droplet to initiate nucleation. The test chamber was held at $1\text{ }^\circ\text{C}$ for 4 h prior to conducting adhesion force measurements.

Adhesion Force Measurement. The adhesive force between the sample and hydrate was measured using the deflection of a cantilevered steel wire, similar to methods previously described elsewhere.¹¹ After the hydrate had fully formed on the surface, the bottom end of a thin wire was brought alongside the hydrate. The top end of the wire was fixed to a micromanipulator stage and slowly exerted a force on the hydrate until the hydrate adhesively or cohesively fractured. A DSLR camera (Nikon) with a high-zoom macro lens (Navitar) was used to record a video of the hydrate detachment. Image analysis was used to measure the displacement of the cantilevered wire during the fracture. The adhesion force was calculated from the wire's deflection, material, and geometric properties using classical cantilevered beam deflection equations.¹¹

■ ASSOCIATED CONTENT

Supporting Information

The Supporting Information is available free of charge on the ACS Publications website at DOI: 10.1021/acsami.7b00223.

Water droplets inside the cyclopentane environment at cyclopentane-entrained and water-impaled states on textured FS surfaces (PDF)

High mobility of water drop on an OTS-treated surface inside oil (MOV)

Rapid spreading of cyclopentane on an OTS-treated surface inside water (MOV)

Depinning of cyclopentane on an FS-treated surface inside water showing reduced interactions between cyclopentane and the solid (MOV)

Poor hydrate stiction during its formation from a water droplet placed on an OTS-treated surface inside water (MOV)

Hydrate particle slides on an OTS-treated surface inside cyclopentane (MOV)

■ AUTHOR INFORMATION

Corresponding Author

*E-mail: varanasi@mit.edu.

ORCID

Taylor A. Farnham: 0000-0002-6157-6551

Present Addresses

[†]T.A.F.: 1127 Fierro Dr. Ojai, CA 93023.

[‡]S.B.S.: 1082 Stonecrest Ct, Johnson City, TN 37604.

Author Contributions

The manuscript was written through contributions of all authors. All authors have given approval to the final version of the manuscript. K.K.V. and A.D. designed research. A.D. performed the experiments. A.D., T.A.F., S.B.S., and K.K.V. analyzed the data and wrote the manuscript.

Funding

This research work was funded by Eni S.p.A through the MIT Energy Initiative.

Notes

The authors declare no competing financial interest.

■ ACKNOWLEDGMENTS

We thank Eni for funding the work. We thank Mr. Giuseppe Maddinelli and Mr. Stefano Carminati of Eni for fruitful discussions. We thank CNS - Center for Nanoscale Systems of Harvard University for using their cleanroom facilities to prepare lithographic samples.

■ REFERENCES

- (1) Sloan, E. D.; Koh, C. A. *Clathrate Hydrates of Natural Gases*, 3rd ed.; CRC Press: Boca Raton, 2007.
- (2) Castellani, B.; Morini, E.; Filipponi, M.; Nicolini, A.; Palombo, M.; Cotana, F.; Rossi, F. Clathrate Hydrates for Thermal Energy Storage in Buildings: Overview of Proper Hydrate-Forming Compounds. *Sustainability* **2014**, *6*, 6815–6829.
- (3) Ogoshi, H.; Matsuyama, E.; Miyamoto, M.; Mizukami, T.; Furumoto, N.; Sugiyama, M. Clathrate Hydrate Slurry, CHS Thermal Energy Storage System and Its Applications. In *2010 International Symposium on Next-generation Air Conditioning and Refrigeration Technology*; Tokyo, Japan, 2010.
- (4) Sum, A. K.; Koh, C. A.; Sloan, E. D. Clathrate Hydrates: From Laboratory Science to Engineering Practice. *Ind. Eng. Chem. Res.* **2009**, *48*, 7457–7465.

(5) Richard, P. Deepwater Horizon oil spill of 2010. <https://www.britannica.com/event/Deepwater-Horizon-oil-spill-of-2010> (accessed Mar 6, 2017).

(6) Koh, C. A.; Westacott, R. E.; Zhang, W.; Hirachand, K.; Creek, J. L.; Soper, A. K. Mechanisms of Gas Hydrate Formation and Inhibition. *Fluid Phase Equilib.* **2002**, *194–197*, 143–151.

(7) Gbaruko, B. C.; Igwe, J. C.; Gbaruko, P. N.; Nwokeoma, R. C. Gas Hydrates and Clathrates: Flow Assurance, Environmental and Economic Perspectives and the Nigerian Liquefied Natural Gas Project. *J. Pet. Sci. Eng.* **2007**, *56*, 192–198.

(8) Bollavaram, P.; Devarakonda, S.; Selim, M. S.; Sloan, E. D. Growth Kinetics of Single Crystal sII Hydrates Elimination of Mass and Heat Transfer Effects. *Ann. N. Y. Acad. Sci.* **2000**, *912*, 533–543.

(9) Dyadin, Y.; Bondaryuk, I.; Aladko, L. Stoichiometry of Clathrates. *J. Struct. Chem.* **1995**, *36*, 995–1045.

(10) Wilson, P. W.; Lester, D.; Haymet, A. D. J. Heterogeneous Nucleation of Clathrates from Supercooled Tetrahydrofuran (THF)/water Mixtures, and the Effect of an Added Catalyst. *Chem. Eng. Sci.* **2005**, *60*, 2937–2941.

(11) Nicholas, J. W.; Dieker, L. E.; Sloan, E. D.; Koh, C. A. Assessing the Feasibility of Hydrate Deposition on Pipeline walls—Adhesion Force Measurements of Clathrate Hydrate Particles on Carbon Steel. *J. Colloid Interface Sci.* **2009**, *331*, 322–328.

(12) Aspenes, G.; Dieker, L. E.; Aman, Z. M.; Høiland, S.; Sum, A. K.; Koh, C. A.; Sloan, E. D. Adhesion Force between Cyclopentane Hydrates and Solid Surface Materials. *J. Colloid Interface Sci.* **2010**, *343*, 529–536.

(13) Aman, Z. M.; Dieker, L. E.; Aspenes, G.; Sum, A. K.; Sloan, E. D.; Koh, C. A. Influence of Model Oil with Surfactants and Amphiphilic Polymers on Cyclopentane Hydrate Adhesion Forces. *Energy Fuels* **2010**, *24*, 5441–5445.

(14) Aman, Z. M.; Brown, E. P.; Sloan, E. D.; Sum, A. K.; Koh, C. A. Interfacial Mechanisms Governing Cyclopentane Clathrate Hydrate Adhesion/cohesion. *Phys. Chem. Chem. Phys.* **2011**, *13*, 19796–19806.

(15) Smith, J. D.; Meuler, A. J.; Bralover, H. L.; Venkatesan, R.; Subramanian, S.; Cohen, R. E.; McKinley, G. H.; Varanasi, K. K. Hydrate-Phobic Surfaces: Fundamental Studies in Clathrate Hydrate Adhesion Reduction. *Phys. Chem. Chem. Phys.* **2012**, *14*, 6013–6020.

(16) Aman, Z. M.; Leith, W. J.; Grasso, G. A.; Sloan, E. D.; Sum, A. K.; Koh, C. A. Adhesion Force between Cyclopentane Hydrate and Mineral Surfaces. *Langmuir* **2013**, *29*, 15551–15557.

(17) Aman, Z. M.; Sloan, E. D.; Sum, A. K.; Koh, C. A. Adhesion Force Interactions between Cyclopentane Hydrate and Physically and Chemically Modified Surfaces. *Phys. Chem. Chem. Phys.* **2014**, *16*, 25121–25128.

(18) Lee, W.; Baek, S.; Kim, J.-D.; Lee, J. W. Effects of Salt on the Crystal Growth and Adhesion Force of Clathrate Hydrates. *Energy Fuels* **2015**, *29*, 4245–4254.

(19) Sojoudi, H.; Walsh, M. R.; Gleason, K. K.; McKinley, G. H. Investigation into the Formation and Adhesion of Cyclopentane Hydrates on Mechanically Robust Vapor-Deposited Polymeric Coatings. *Langmuir* **2015**, *31*, 6186–6196.

(20) Morrissy, S. A.; Lim, V. W.; May, E. F.; Johns, M. L.; Aman, Z. M.; Graham, B. F. Micromechanical Cohesive Force Measurements between Precipitated Asphaltene Solids and Cyclopentane Hydrates. *Energy Fuels* **2015**, *29*, 6277–6285.

(21) Karanjkar, P. U.; Lee, J. W.; Morris, J. F. Surfactant Effects on Hydrate Crystallization at the Water-Oil Interface: Hollow-Conical Crystals. *Cryst. Growth Des.* **2012**, *12*, 3817–3824.

(22) Hejda, F.; Solar, P.; Kousal, J. Surface Free Energy Determination by Contact Angle Measurements: A Comparison of Various Approaches. *WDS'10 Proceedings of Contributed Papers; Part III* **2010**, pp 25–30.

(23) Pauling, L. Nature of the Chemical Bond [Russian Translation]; Goskomisdat: Moscow, 1947; p 206.

(24) Ishino, C.; Okumura, K. Wetting Transitions on Textured Hydrophilic Surfaces. *Eur. Phys. J. E: Soft Matter Biol. Phys.* **2008**, *25*, 415–424.

(25) Smith, J. D.; Dhiman, R.; Anand, S.; Reza-Garduno, E.; Cohen, R. E.; McKinley, G. H.; Varanasi, K. K. Droplet Mobility on Lubricant-Impregnated Surfaces. *Soft Matter* **2013**, *9*, 1772–1780.

(26) Van Oss, C. J.; Good, R. J.; Chaudhury, M. K. Additive and Nonadditive Surface Tension Components and the Interpretation of Contact Angles. *Langmuir* **1988**, *4*, 884–891.

(27) Good, R. J. Contact Angle, Wetting, and Adhesion: A Critical Review. *J. Adhes. Sci. Technol.* **1992**, *6*, 1269–1302.